Heliyon 5 (2019) e02257

Contents lists available at ScienceDirect

Heliyon

journal homepage: www.heliyon.com

Cancer stem cell subpopulations in moderately differentiated head and neck cutaneous squamous cell carcinoma☆

Sabrina P. Koh [a], Helen D. Brasch [a], Jennifer de Jongh [a], Tinte Itinteang [a,1], Swee T. Tan [a,b,*,1]

[a] Gillies McIndoe Research Institute, New Zealand
[b] Wellington Regional Plastic, Maxillofacial & Burns Unit, Hutt Hospital, Wellington, New Zealand

ARTICLE INFO

Keywords:
Cancer research
Cutaneous
Head and neck
Cancer
Stem cell
Squamous cell carcinoma
Hierarchy

ABSTRACT

Cancer stem cells (CSC), the putative origin of cancer, account for local recurrence and metastasis. We aimed to identify and characterize CSCs within moderately differentiated head and neck cutaneous squamous cell carcinoma (MDHNCSCC).

Formalin-fixed paraffin-embedded MDHNCSCC sections of ten patients underwent 3,3-diaminobenzidine (DAB) immunohistochemical (IHC) staining for induced pluripotent stem cell (iPSC) markers OCT4, NANOG, SOX2, KLF4 and c-MYC. Localization of these markers was investigated using immunofluorescence (IF) IHC staining of three of these MDHNCSCC samples. mRNA expression of these iPSC markers in the MDHNCSCC tissue samples was determined by colorimetric *in-situ* hybridization (CISH, n = 6), and reverse-transcription quantitative polymerase chain reaction (RT-qPCR, n = 4). RT-qPCR was also performed on four MDHNCSCC-derived primary cell lines.

DAB IHC staining demonstrated expression of all five iPSC markers within all ten MDHNCSCC tissues samples. CISH and RT-qPCR confirmed mRNA expression of all five iPSC markers within all MDHNCSCC tissues samples examined. RT-PCR demonstrated mRNA transcripts of all five iPSC markers in all four MDHNCSCC-derived primary cell lines.

IF IHC staining showed co-expression of OCT4 with SOX2 and KLF4 throughout the tumor nests (TNs) and peritumoral stroma (PTS). There was an $OCT4^+/NANOG^+$ subpopulation within the TNs, and an $OCT4^+/NANOG^-$ subpopulation and an $OCT4^+/NANOG^+$ subpopulation within the PTS. All iPSC markers were expressed by the endothelium of microvessels within the PTS.

Our findings suggest the presence of an $OCT4^+/NANOG^+/SOX2^+/KLF4^+/c\text{-}MYC^+$ CSC subpopulation within the TNs, PTS and endothelium of microvessels within the PTS; and an $OCT4^+/NANOG^-/SOX2^+/KLF4^+/c\text{-}MYC^+$ subpopulation exclusively within the PTS in MDHNCSCC. These CSC subpopulations could be a potential novel therapeutic target for treatment of MDHNCSCC.

1. Introduction

Cutaneous squamous cell carcinoma (cSCC) accounts for 15–25% of non-melanoma skin cancers [1, 2, 3, 4, 5]. A 3-fold increase in the incidence of cSCC has been observed over the past three decades [6]. Non-modifiable predisposing factors for cSCC include pale complexion that is associated with a 2–5 fold increased risk, Caucasian descent, and increasing age [2, 3, 7]. Ultraviolet (UV) radiation has a prominent role in the development of SCC, with UV specific point mutations in the p53 tumor suppressor gene, which are typically absent in malignancies arising in non-sun exposed sites, being observed in SCC [8].

Approximately 1.9–2.6% of cSCC develop metastasis [1], at a mean of 26 months from diagnosis [1]. 85% of metastases occur in the regional lymph nodes, most commonly the parotid and/or the neck [7], which is

☆ Aspects of this work was presented at the Royal Australasian College of Surgeons' 87th Annual Scientific Congress with the American College of Surgeons and the Australian and New Zealand College of Anaesthetists' Annual Scientific Meeting, Sydney, Australia, May 7–11, 2018; and the 20th Annual Meeting of the Australian and New Zealand Head and Neck Cancer Society and the 15th Meeting of the International Society for Maxillofacial Rehabilitation, Melbourne, Australia, July 26–28, 2018.

* Corresponding author.
E-mail address: swee.tan@gmri.org.nz (S.T. Tan).

[1] equal senior authors.

https://doi.org/10.1016/j.heliyon.2019.e02257
Received 30 March 2019; Received in revised form 26 July 2019; Accepted 5 August 2019

associated with a 5-year survival of 48% [9], and 10-year survival of less than 20% [7], despite intensive treatment. Factors associated with an increased risk of metastasis include perineural invasion [1, 6, 7], lymphovascular invasion [1, 6], poor histological differentiation [1, 6, 7, 10], certain anatomic subsites such as the ear [1, 6, 7], tumor thickness of >2mm [6, 10] and horizontal tumor diameter of >2cm [6, 7]. Surgical excision is the mainstay treatment [2, 11] for cSCC, with adjuvant radiotherapy for advanced cases [12].

The hierarchical model of cancer proposes the presence of a small subpopulation of highly tumorigenic cancer stem cells (CSCs) within a tumor. These CSCs are functionally analogous to embryonic stem cells (ESCs), and are imbued with the capacity for uncontrolled growth, self-renewal, and pluripotency [13, 14, 15]. CSCs undergo asymmetric division to replenish the CSC population and give rise to progenitor cancer cells, which subsequently differentiate into mature, non-tumorigenic cancer cells [13, 14, 16]. Furthermore, CSCs are resistant to chemotherapy and radiotherapy, and are the suggested source of local recurrence and metastasis [15, 16, 17]. These CSCs sit at the apex of a putative hierarchy, reminiscent of normal ESCs, with the expression of various stem cell markers characterizing cells at different stages in this hierarchy [13, 16].

While numerous markers have been used to profile CSCs, certain markers, particularly ESC-associated markers OCT4, NANOG, SOX2, KLF4 and c-MYC have been used to characterize CSCs in solid tumors [18, 19, 20, 21], and they may have a more pronounced role in promoting stemness and driving tumorigenesis [22].

OCT4 plays a central role in regulating pluripotency, with positive correlations between OCT4 expression and poor prognosis observed in several malignancies, including head and neck SCC (HNSCC) [23]. Increased expression of OCT4 has been shown to be positively correlated with upregulation of stem cell traits, including increased self-renewal, chemo-resistance and potential for migration and invasion, with OCT4 gene knockout resulting in reduced cell viability and self-renewal capacity, following chemotherapy [23]. Studies have demonstrated the crucial role of OCT4 in promoting the stem-cell phenotype [23, 24]. Racila *et al.* [24] demonstrate transient transfection of human keratinocytes with OCT4, is sufficient to promote de-differentiation of these cells into a more primitive mesenchymal state, with cells transfected with OCT4 subsequently also expressing SOX2 and NANOG. Similarly, Koo *et al.* [23] demonstrate that the presence of OCT4 promotes de-differentiation of mature HNSCC cells into a primitive stem cell-like state.

SOX2 possesses oncogenic properties, with upregulation paralleled by an increase in expression of genes implicated in cell proliferation and maintenance of stemness [25]. Furthermore, deletion of SOX2 in human SCC cell line derived tumors in xenotransplanted mice models, results in tumor regression [25]. OCT4, SOX2 and NANOG appear to have a synergistic roles in inducing and maintaining pluripotency [22, 23, 24].

The precise role of KLF4 in tumorigenesis is less well defined, but has been shown to be upregulated in human SCC tissues when compared to surrounding non-tumor peri-tumoral tissue [26]. The presence of KLF4 is thought to contribute to the initiation of epithelial dysplasia, with Foster *et al.* [27] demonstrating that induction of KLF4 in basal keratinocytes of transgenic mice, promotes the formation of dysplastic lesions bearing morphologic and molecular parallels to human cSCC.

Activation of the c-MYC protooncogene in epidermal cells in murine models results in promotion of proliferation and prevention of differentiation [28]. Furthermore, c-MYC expression promotes angiogenesis and appears to suppress apoptosis [28].

Interestingly, studies have shown that transduction of these five ESC markers OCT4, NANOG, SOX2, KLF4 and c-MYC, into somatic cells, has the capacity to cause these cells to enter into a primitive pluripotent state, termed induced pluripotent stem cells (iPSC) [29, 30].

This study identified and characterized the CSC population within moderately differentiated head and neck CSCC (MDHNcSCC), using the iPSC markers OCT4, NANOG, SOX2, KLF4 and c-MYC at both the transcriptional and translational levels.

2. Materials and methods

2.1. MDHNcSCC tissue samples

MDHNcSCC tissue samples from 9 male and 1 female patients, aged 60–93 (mean, 77.3) years, were sourced from the Gillies McIndoe Research Institute Tissue Bank for this study, which was approved by the Central Regional Health and Disability Ethics Committee (Ref. 12/CEN/74). Written informed consent was obtained from all patients included in this study.

2.2. MDHNcSCC-derived primary cell lines

MDHNcSCC-derived primary cell lines were derived from four fresh surgically excised MDHNcSCC tissue samples of the original cohort of ten patients included in 3,3-diaminobenzidine (DAB) immunohistochemical (IHC) staining, by culturing them within a Matrigel explant and then extracting the cells following abundant growth, as previously described [31]. The extracted HNCSCC cells were cultured and passaged in DMEM medium (cat# 10569010, Gibco, Thermo Fisher Scientific, Waltham, MA, USA) supplemented with 1% FCS (cat# 10091148, Gibco, Thermo Fisher Scientific), 5% mTeSR™ (cat# 85850, StemCell Technologies, Vancouver, BC, Canada), 1% penicillin-streptomycin (cat# 15140122, Gibco, Thermo Fisher Scientific) and 0.2% gentamicin/amphotericin B (cat# R01510, Gibco, Thermo Fisher Scientific). All cultures were maintained in a humidified incubator at 37 °C with an atmosphere of 94% air and 5% CO_2. All primary cell lines used for the experiments were between passages 6–8.

2.3. Histochemical and immunohistochemical staining

4μm-thick formalin-fixed paraffin-embedded sections of MDHNcSCC tissue samples from ten patients were subjected to hematoxylin & eosin (H&E) staining to confirm the diagnosis and histological grade of the MDHNcSCC by an anatomical pathologist (HDB). The same MDHNcSCC tissue samples were subjected to DAB IHC staining, as previously described [32], using the Leica Bond Rx auto-stainer (Leica, Nussloch, Germany), with primary antibodies: c-MYC (1:1000; cat# ab32, Abcam, Cambridge, MA, USA), KLF4 (1:100; cat# nBP2-24749, Novus Biologicus, Littleton, CO, USA), NANOG (1:200; cat# EP225, Cell Marque, Rocklin, Ca, USA), OCT4 (1:30; cat# MRQ-10, Cell Marque) and SOX2 (1:500; cat# PA1-094, Thermo Fisher Scientific). All antibodies were diluted with Bond™ primary antibody diluent (cat# AR9352, Leica). DAB IHC-stained slides were mounted in Surgipath Micromount mounting medium (cat# 38017322, Leica).

Three representative MDHNcSCC tissue samples from the original cohort of ten patients included in DAB IHC staining were subjected to immunofluorescence (IF) IHC staining as previously described [32]. Staining was performed using identical primary antibodies and concentrations as used for DAB IHC staining of the ESC markers. Dual staining of the iPSC markers with primary antibodies for endothelial markers CD34 (ready-to-use; cat# PA0212, Leica) and ERG (1:200; cat# EP111, Cell Marque) was performed to determine their expression on the endothelium. Primary antibodies were detected using an appropriate fluorescent secondary antibody of either Vectafluor Excel anti-mouse (ready-to-use; cat# VEDK2488, Vector Laboratories, Burlingame, CA, USA) or Alexa Fluor anti-rabbit 594 (1:500; cat# A21207, Life Technologies, Carlsbad, CA, USA). IF IHC-stained slides were mounted in Vectashield HardSet anti-fade mounting medium and counter-stained with 4′6-diamino-2-phenylinodole (cat# H-1500, Vector Laboratories).

Positive human control tissues used were prostate for c-MYC, breast carcinoma for KLF4, seminoma for NANOG and OCT4, and skin for SOX2. To determine the specificity of the amplification cascade used in DAB IHC staining, negative controls were performed on sections of

MDHNcSCC using a matched isotype control for both mouse (ready-to-use; cat# IR750, Dako, Copenhagen, Denmark) and rabbit (ready-to-use; cat# IR600, Dako) primary antibodies, and a combination of both for IF IHC staining.

2.4. Colorimetric in-situ hybridization

4μm-thick formalin-fixed paraffin-embedded sections of six MDHNcSCC tissue samples from the original cohort of ten patients included in DAB IHC staining were subject to colorimetric *in-situ* hybridization (CISH) analysis. Staining was performed using the Leica Bond Rx autostainer with probes for c-MYC (NM_002467.4), KLF4 (NM_001314052), NANOG (NM_024865.2), OCT4 (NM002701.4) and SOX2 (NR_075091.1). All probes used for CISH were obtained from Advanced Cell Diagnostics (Newark, CA, USA). Probes were detected using the RNAscope 2.5 LS Reagent Brown Kit (cat# 322100, Advanced

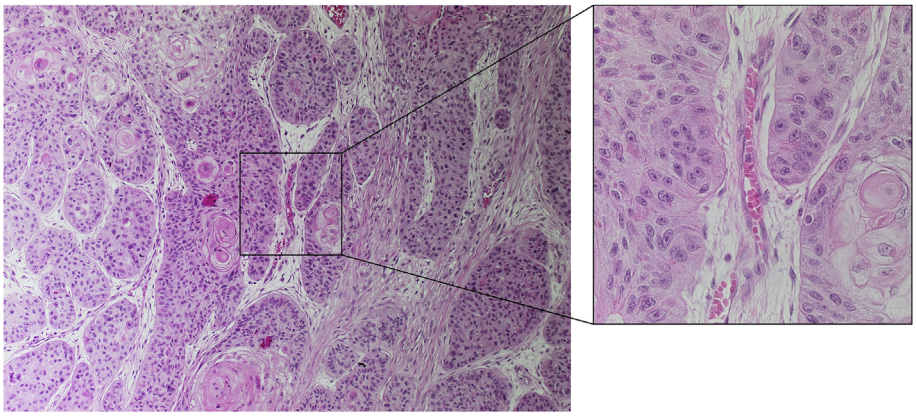

Fig. 1. A representative hematoxylin and eosin stained slide of a moderately differentiated head and neck cutaneous squamous cell carcinoma tissue sample demonstrating the presence of islands of tumor nests (TNs) surrounded by peritumoral stroma (PTS) which contained microvessels. A magnified view showing a microvessel within the PTS within the box. Original magnification: 400x.

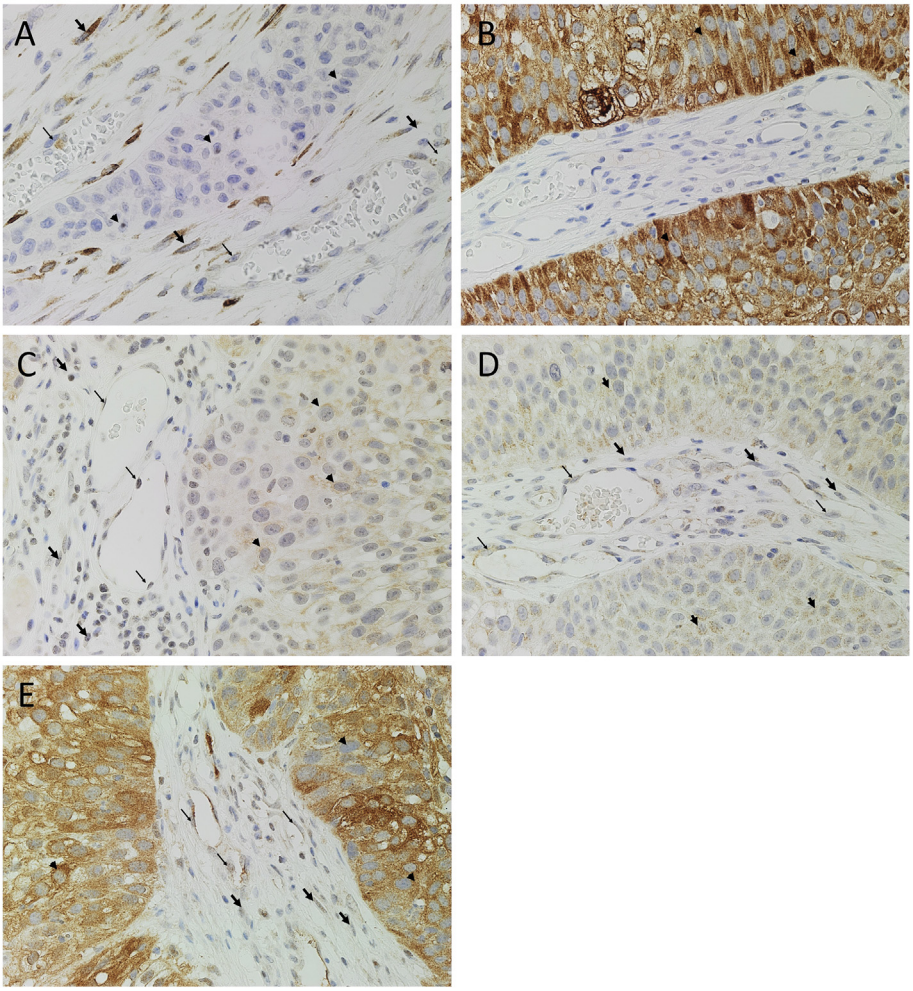

Fig. 2. Representative 3,3-diaminobezidine immunohistochemical-stained slides of moderately differentiated head and neck cutaneous squamous cell carcinoma tissue samples demonstrating the expression of OCT4 (A, brown), NANOG (B, brown), SOX2 (C, brown), KLF4 (D, brown) and c-MYC (E, brown) by cells within the tumor nests (*arrowheads*), the peritumoral stroma (PTS, *thick arrows*), and the endothelium of microvessels (*thin arrows*) within the PTS. Nuclei were counter-stained with hematoxylin (A-F, blue). Original magnification: 400x.

Cell Diagnostics). Positive human controls were demonstrated on sections of seminoma for OCT4, NANOG and SOX2; prostate for c-MYC; and breast carcinoma. Negative controls were demonstrated on sections of MDHNcSCC using a probe for DapB (EF191515) (cat# 3120358, Advanced Cell Diagnostics).

2.5. Image analysis

DAB IHC-stained and CISH-stained slides were visualized and imaged using an Olympus BX53 light microscope fitted with an Olympus SC100 digital camera, and processed with the CellSens 2.0 Software (Olympus, Tokyo, Japan). IF IHC-stained slides were viewed and imaged with an Olympus FV1200 biological confocal laser-scanning microscope and subjected to 2D deconvolutional processing with CellSens Dimension 1.11 software (Olympus).

2.6. Reverse-transcription quantitative polymerase chain reaction

RNA was extracted from 20mg sections of four snap-frozen MDHNcSCC tissue samples from the original cohort of ten patients included for DAB IHC staining. Tissue sections were individually suspended in 350μL lysis buffer RLT (cat# 79216, Qiagen, Hilden, Germany). Samples were homogenized using the Omni Tissue Homogenizer (Omni International, Kennesaw, GA, USA). Homogenised samples were prepared using the RNeasy Mini Kit (Qiagen), with RNA extracted using the QIAcube (Qiagen). Samples were then subjected to NanoDrop 2000 Spectrophotometer (ThermoFisher Scientific) quantification. Extractions for each sample were performed in triplicates and analyzed.

Similarly, primary cell lines derived from four fresh MDHNcSCC tissue samples of the original cohort of ten patients included in DAB IHC staining, were subjected to the same RNA extraction process.

RNA extracted from the four snap-frozen MDHNcSCC tissue samples and the four MDHNcSCC-derived primary cell lines were prepared with Rotor-Gene Multiplex RT-PCR Kit (Qiagen), and subjected to RT-qPCR using the Rotor-Gene Q (Qiagen), with probes for SOX2 (Hs01053049_s1), KLF4 (Hs00358836_m1), NANOG (Hs04399610_g1), OCT4 (Hs00999632_g1), c-MYC (Hs00153408_m1) and the housekeeping gene GAPDH (Hs99999905_m1). All primers were obtained from Thermo Fisher Scientific.

Positive controls were demonstrated on PC3 cell lines, and specificity of probes confirmed by inclusion of a water negative control.

To confirm the specificity of the PCR reaction, 1% precast agarose gels (cat# G401001, Thermo Fisher Scientific) were loaded with products of the PCR reactions, alongside a 1Kb ladder (cat# 10488090, Thermo Fisher Scientific). Electrophoresis was performed using the eGel equipment (cat# G6400, Thermo Fisher Scientific). All gels were imaged using the ChemiDoc MP (Bio-rad).

3. Results

3.1. Histochemical and 3,3-diaminobenzidine immunohistochemical staining

The diagnosis and appropriate histological grade were confirmed on H&E stained sections of all ten MDHNcSCC tissue samples (Fig. 1). DAB IHC-stained sections of the same ten MDHNcSCC tissue samples

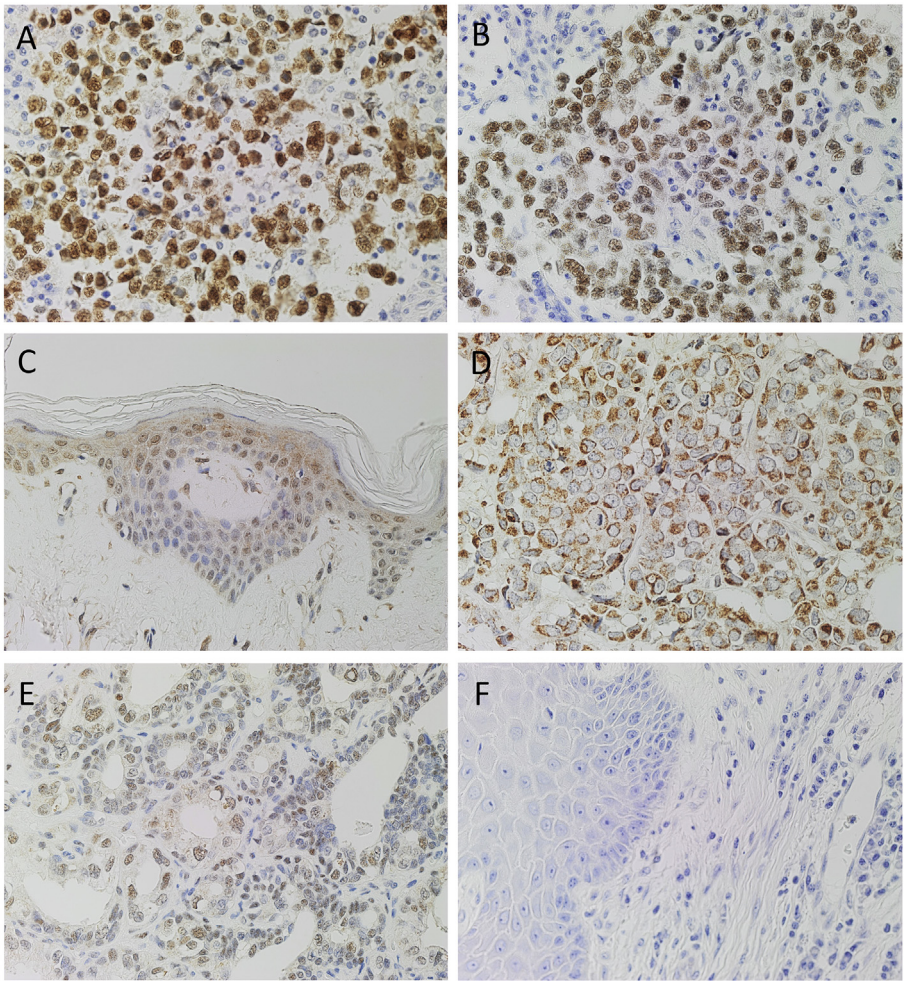

Fig. 3. Positive 3,3-diaminobezidine immunohistochemical-stained of human control tissues: seminoma confirming the expression of OCT4 (A, brown) and NANOG (B, brown), normal skin for SOX2 (C, brown), breast carcinoma for KLF4 (D, brown) and prostate tissue for c-MYC (E, brown). A section moderately differentiated head and neck cutaneous squamous cell carcinoma probed with a matched isotype control for mouse and primary antibodies (F, brown), confirmed specificity of the secondary antibodies. Nuclei were counter-stained with hematoxylin (A-F, blue). Original magnification: 400x.

demonstrated the expression of OCT4 (Fig. 2A, brown) by cells within the peritumoral stroma (PTS, *thick arrows*), weak staining on cells within the tumor nests (TNs, *arrowheads*) and the endothelium of the microvessels within the PTS (*thin arrows*). NANOG (Fig. 2B, brown) was exclusively expressed on the cytoplasm of cells within the TNs (*arrowheads*). SOX2 (Fig. 2C, brown) was expressed homogenously in the cytoplasm of cells within the TNs *(arrowheads*), with a small subpopulation also showing nuclear expression. Nuclear and cytoplasmic expression of SOX2 was present on the endothelium of microvessels (*thin arrows*) and some cells within the PTS (*thick arrows*). Cytoplasmic expression of KLF4 (Fig. 2D, brown) was observed in cells throughout the TNs (*arrowheads*), PTS (*thick arrows*) and endothelium of microvessels (*thin arrows*) within the PTS. Cells within the TNs (*arrowheads*) exhibited ubiquitous cytoplasmic and occasional nuclear expression of c-MYC (Fig. 2E, brown). Nuclear and cytoplasmic expression of c-MYC was seen on the endothelium of the microvessels (*thin arrows*) and in a small number of cells within the PTS (*thick arrows*).

Positive staining was demonstrated on sections of human tissues: seminoma for OCT4 (Fig. 3A, brown) and NANOG (Fig. 3B, brown), skin for SOX2 (Fig. 3C, brown), breast carcinoma for KLF4 (Fig. 3D, brown) and prostate for c-MYC (Fig. 3E, brown). Specificity of staining was confirmed on sections of MDHNcSCC tissues using a matched isotype control for both mouse and rabbit primary antibodies (Fig. 3F).

3.2. Immunofluorescence immunohistochemical staining

IF IHC staining demonstrated abundant expression of OCT4 (Fig. 4A-C, green) on cells within the PTS (*arrows*) and weak cytoplasmic expression on cells within the TNs (*arrowheads*). The $OCT4^{+}$ subpopulations within the TNs (*arrowheads*) and the PTS (*arrows*) also exhibited nuclear and cytoplasmic expression of SOX2 (Fig. 4A, red). The $OCT4^{+}$ cells within the TNs further demonstrated homogenous expression of NANOG (Fig. 4B, red, *arrowheads*). There was an $OCT4^{+/}NANOG^{+}$ subpopulation (*thick arrows*) and an $OCT4^{+}/NANOG^{-}$ subpopulation (*thin arrows*) within the PTS. The $OCT4^{+}$ subpopulations within the TNs (*arrowheads*) and PTS (*arrows*) demonstrated nuclear and cytoplasmic expression of KLF4 (Fig. 4C, red). The $SOX2^{+}$ (Fig. 4D, red) cells within both the TNs (*arrowheads*) and PTS (*arrows*) also expressed c-MYC (Fig. 4D, green). Dual staining of the iPSC markers with endothelial markers CD34 (Fig. 4E-G, green) or ERG (Fig. 4H-I, red) demonstrated expression of SOX2 (Fig. 4E, red), NANOG (Fig. 4F, red), KLF4 (Fig. 4G, red), OCT4 (Fig. 4H, green) and c-MYC (Fig. 4I, green) on the endothelium of microvessels (*arrows*) within the PTS.

Images demonstrating individual stains of the merged images illustrated in Fig. 4 are provided in Fig. 5. Specificity of primary antibodies was confirmed on the negative control (Fig. 5S), which demonstrated minimal staining.

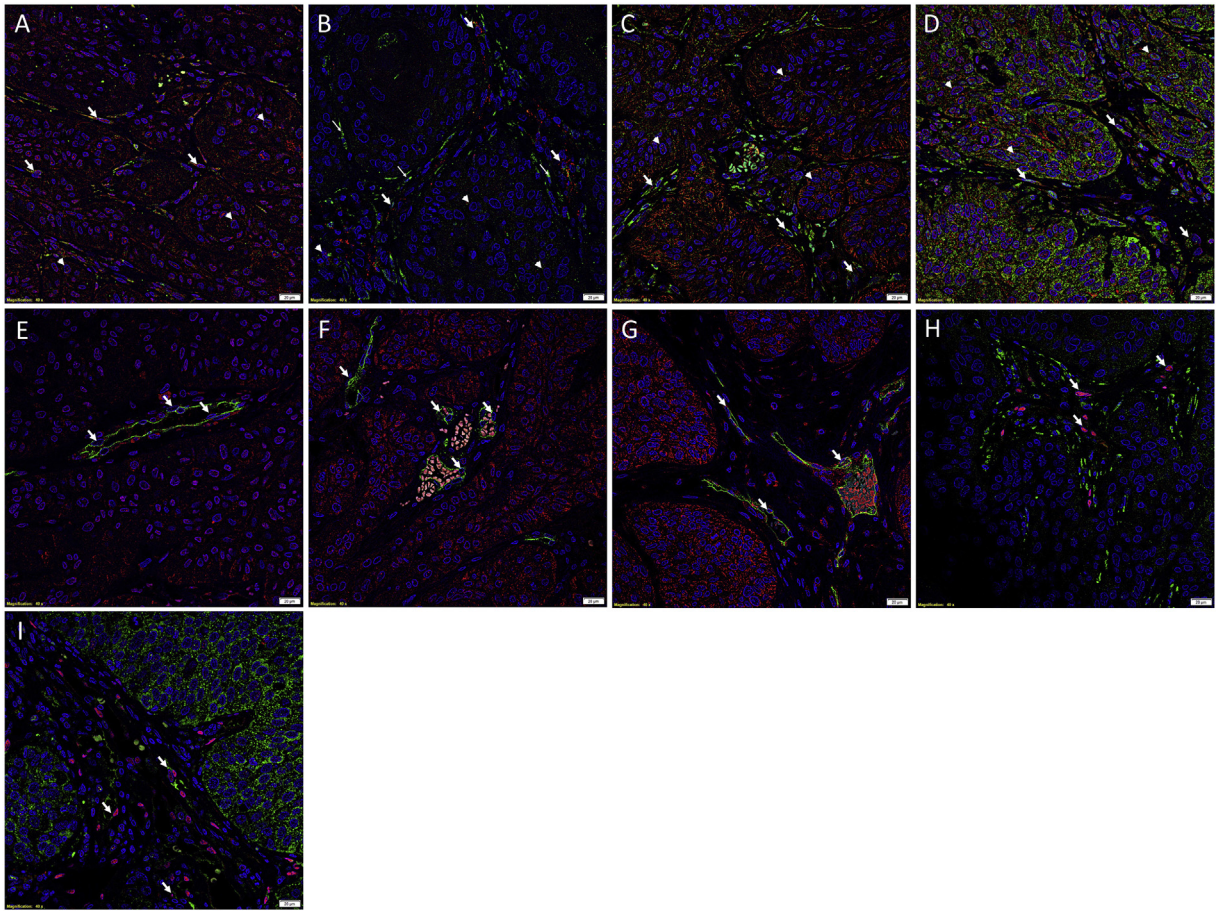

Fig. 4. Representative immunofluorescence immunohistochemical-stained sections of moderately differentiated head and neck cutaneous squamous cell carcinoma tissue samples demonstrating expression of OCT4 (A-C, green) on cells within the peri-tumoral stroma (PTS, *arrows*) and weak cytoplasmic expression on cells within the TNs (*arrowheads*). The $OCT4^{+}$ subpopulations in the tumor nests (TNs, *arrowheads*) and the PTS (*arrows*) also exhibited nuclear and cytoplasmic expression of SOX2 (A, red). The $OCT4^{+}$ cells within the TNs (*arrowhead*) further demonstrated homogenous expression of NANOG (B, red). There was an $OCT4^{+/}NANOG^{+}$ subpopulation (*thick arrows*) and an $OCT4^{+}/NANOG^{-}$ subpopulation (*thin arrows*) within the PTS. The $OCT4^{+}$ subpopulations within the TNs (*arrowheads*) and PTS (*arrows*) demonstrated nuclear and cytoplasmic expression of KLF4 (C, red). The $SOX2^{+}$ (D, red) cells within both the TNs (*arrowheads*) and the PTS (*arrows*) also expressed c-MYC (D, green). Dual staining of the iPSC markers with endothelial markers CD34 (E-G, green) or ERG (H–I, red) demonstrated expression of SOX2 (E, red), NANOG (F, red), KLF4 (G, red), OCT4 (H, green) and c-MYC (I, green) on the endothelium of microvessels (*arrows*) within the PTS. All slides were counter-stained with 4′,6′-diamino-2-phenylindole. Scale bars: 20μm.

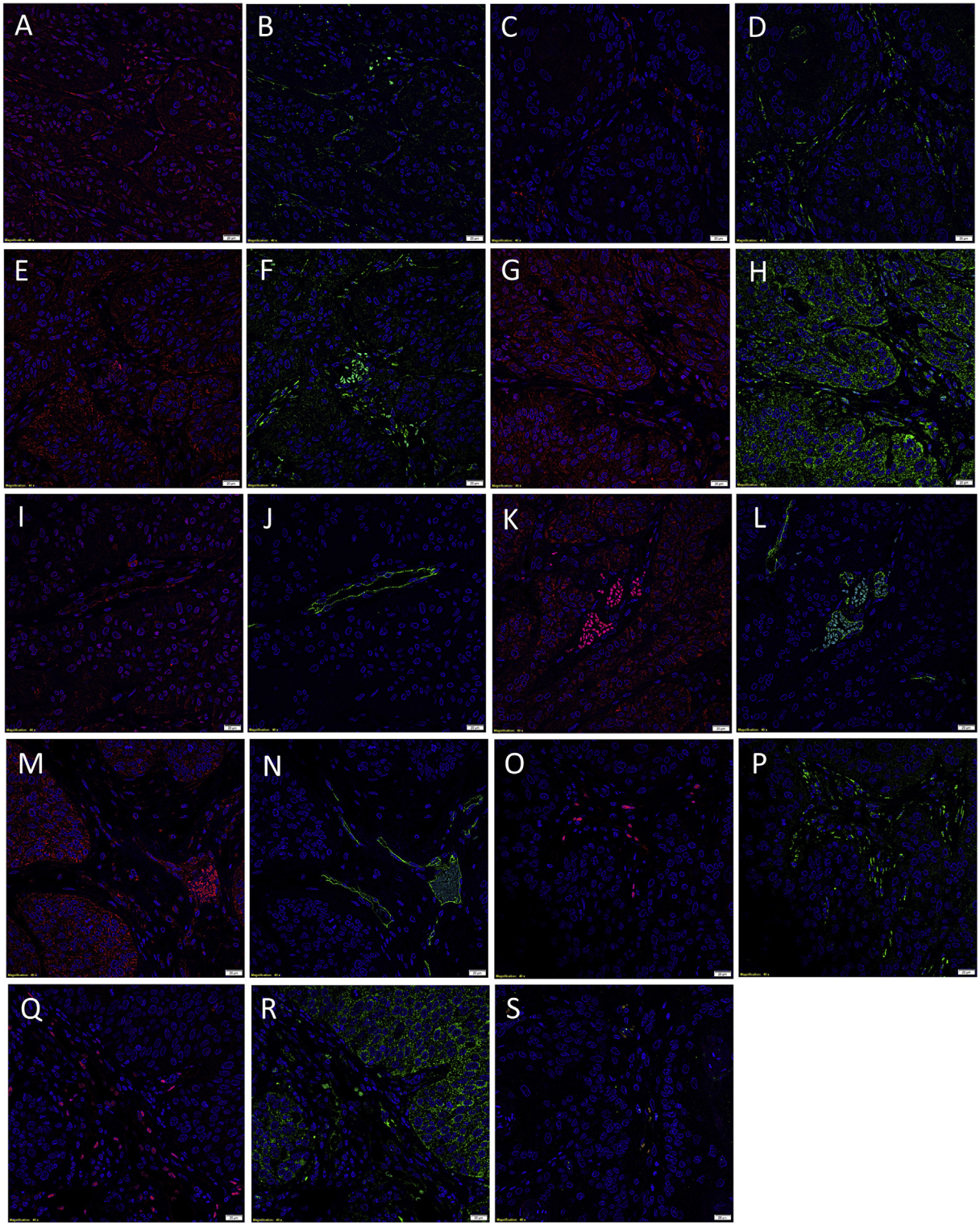

Fig. 5. Individual stains of immunofluorescence immunohistochemical stains of moderately differentiated head and neck cutaneous squamous cell carcinoma (MDHNcSCC) sections shown in Fig. 2. Sections co-stained for OCT4 (B,D,F, green) and SOX2 (A, red), NANOG (C, red) and KLF4 (E, red); and SOX2 (G, red) and c-MYC (H, green). Localization to the endothelium of the microvessels was demonstrated by sections co-stained with CD34 (J,L,N, green) and SOX2 (I, red), NANOG (K, red) and KLF4 (M, red); and ERG (O,Q, red) and OCT4 (P, green) and c-MYC (R, green). A negative control (S), confirming the specificity of the fluorescent secondary antibodies is demonstrated on a section of MDHNcSCC tissue sample. Cell nuclei were counter-stained with 4′6-diamino-2-phenylinodole (Q–S). Scale bars: 20μm.

3.3. Colorimetric in-situ hybridization

CISH demonstrated abundant expression of mRNA transcripts for OCT4 (Fig. 6A, brown), NANOG (Fig. 6B, brown), SOX2 (Fig. 6C, brown), KLF4 (Fig. 6D, brown) and c-MYC (Fig. 6E, brown) throughout the TNs (Fig. 6A-E, *arrowheads*), and to a lesser extent, within the PTS (Fig. 6A-E, *thick arrows*) and endothelium (Fig. 6A-E, *thin arrows*) of microvessels within the PTS. The positive and negative controls for the probes are provided in Fig. 7.

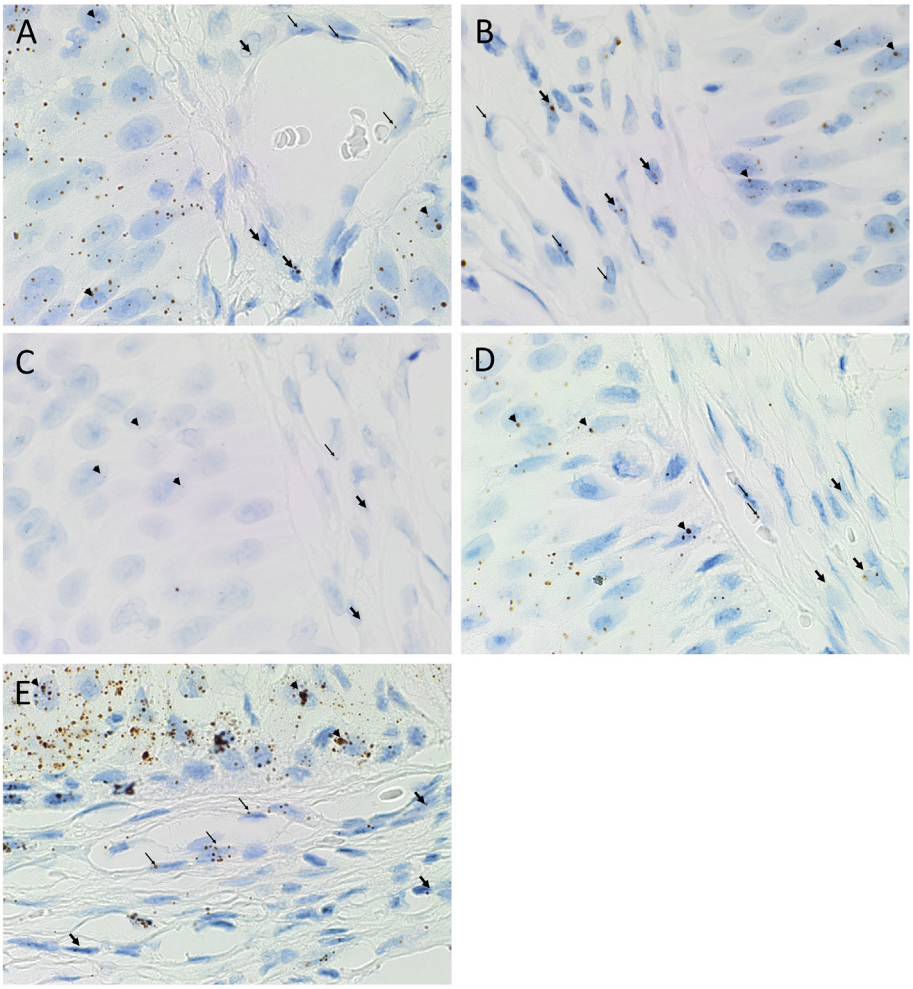

Fig. 6. Representative moderately differentiated head and neck cutaneous squamous cell carcinoma tissue samples subjected to colorimetric *in-situ* hybridization demonstrating expression of OCT4 (A, brown), NANOG (B, brown), SOX2 (C, brown), KLF4 (D, brown) and c-MYC (E, brown) in the tumor nests (*arrowheads*), the peri-tumoral stroma (PTS, *thick arrows*), and the endothelium of microvessels (*thin arrows*) within the PTS. Nuclei were counter-stained with hematoxylin (A-E, blue). Original magnification: 1000x.

3.4. Reverse-transcription quantitative polymerase chain reaction

Reverse-transcription quantitative polymerase chain reaction (RT-qPCR) on all four MDHNCSCC tissue samples demonstrated transcriptional activation of OCT4 (Fig. 8A), NANOG (Fig. 8B), SOX2 (Fig. 8C), KLF4 (Fig. 8D) and c-MYC (Fig. 8E), relative to the house keeping gene GAPDH. RT-qPCR of four MDHNcSCC-derived primary cell lines confirmed the presence of mRNA transcripts for OCT4 (Fig. 9A), NANOG (Fig. 9B), SOX2 (Fig. 9C), KLF4 (Fig. 9D) and c-MYC (Fig. 9E) relative to the house keeping gene GAPDH.

4. Discussion

The stochastic model of cancer attributes tumorigenesis to genomic instability, with all cells being susceptible to the cumulative acquisition of genetic mutations. Those that acquire mutations conducive for sustaining tumorigenesis, subsequently undergo aberrant clonal expansion to form the bulk of the tumor [13, 33]. In contrast, the CSC concept of cancer proposes that a small subpopulation of CSCs sits at the apex of a unidirectional hierarchy, reminiscent of that exhibited by normal stem cells. These normally quiescent cells may be recruited sporadically to undergo symmetric division giving rise to more CSCs, and/or divide asymmetrically to form progenitor cancer cells which subsequently differentiate into mature cancer cells [13, 17, 22, 33]. CSCs are thought to be the source of local recurrence and metastasis and could explain intra-tumoral heterogeneity [14, 15, 17].

Our findings suggest the presence of an $OCT4^{+}/NANOG^{+}/SOX2^{+}/KLF4^{+}/cMYC^{+}$ CSC subpopulation within the TNs, the PTS and the endothelium of microvessels within the PTS and an $OCT4^{+}/NANOG^{-}/SOX2^{+}/KLF4^{+}/c\text{-}MYC^{+}$ subpopulation exclusively within the PTS in MDHNcSCC. These findings are consistent with our previous identification of CSC subpopulations localized to the TNs, PTS and endothelium of the microvessels within the PTS, in buccal mucosal [19], lip [18], and oral tongue [20] SCC.

Support for the presence of the iPSC markers identified on IHC staining is supported transcriptionally at the tissue level by both CISH and RT-qPCR. Furthermore, the transcriptional activation of these markers, evident in the MDHNcSCC-derived primary cell lines is exciting and corroborates the aforementioned findings. It is worth noting that the Matrigel scaffold used for initial derivation of the primary derived cell lines is followed by use of mTeSR, with the latter preferentially used during iPSC culture [34, 35]. It is plausible that the culture conditions have either maintained or produced iPSC-like cells. The reported presence of these iPSC factors within the tissue would support the former over the latter, as no transfection of these genes were performed on these primary cell lines, compared to Yamanaka's reprogrammed fibroblasts [29]. However, the proof of this is beyond the scope of this work.

The presence of a CSC hierarchy has been demonstrated in glioblastoma (GB) by genetic lineage tracing assays, and more recently through DNA barcoding [36]. The spectrum of phenotypes exhibited by CSCs,

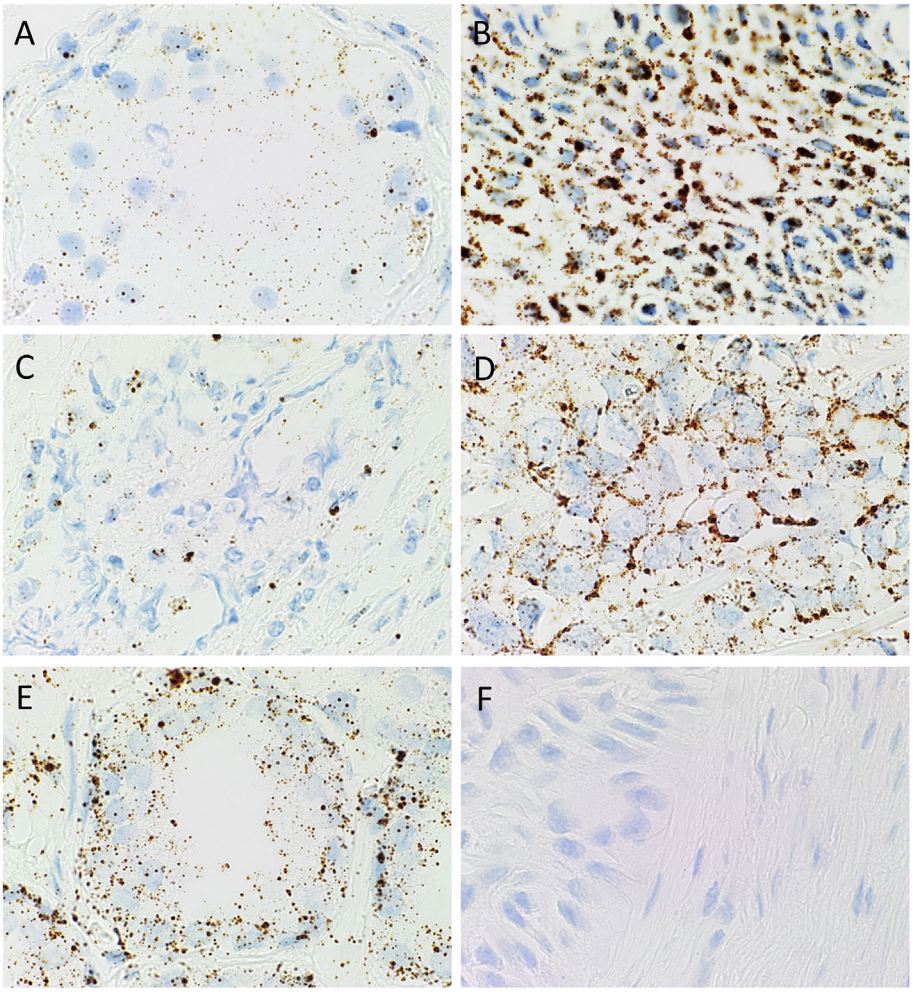

Fig. 7. Positive colorimetric *in-situ* hybridization controls for OCT4 (A), brown, NANOG (B, brown), SOX2 (C), brown) demonstrated on sections of human seminoma tissue. Sections of human breast carcinoma and prostate tissue demonstrating positive staining for KLF4 (D, brown) and c-MYC (E, brown), respectively. Negative control (F) performed on sections of moderately differentiated head and neck cutaneous squamous cell carcinoma tissue sample confirms specificity of secondary antibody. Original magnification: 1000x.

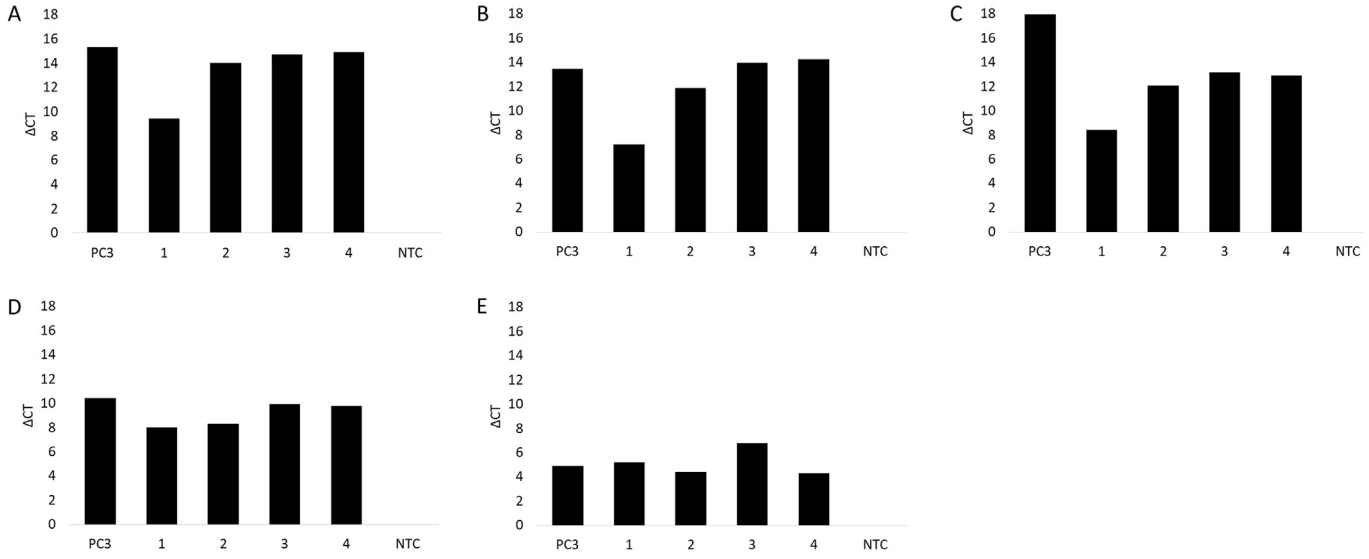

Fig. 8. Graph showing average ΔCT values of triplicate RT-qPCR runs performed on snap-frozen moderately differentiated head and neck cutaneous squamous cell carcinoma tissue samples, amplifying transcripts for OCT4 (A), NANOG (B), SOX2 (C), KLF4 (D) and c-MYC (E). ΔCT was calculated by comparing CT values of induced-pluripotent stem cell markers to that of housekeeping gene GADPH. Positive controls are confirmed using PC3 cells, and specificity of probe is demonstrated using a no template control (NTC).

alludes to the presence of a CSC hierarchy, where only a small subpopulation of these CSCs are 'true' primitive CSCs, while the

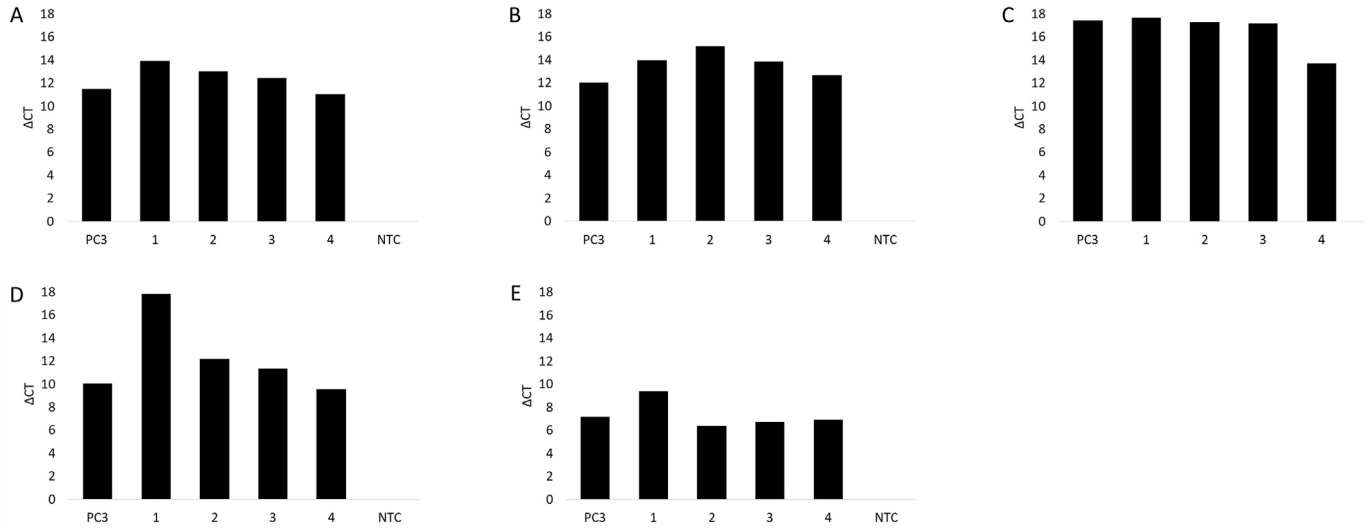

Fig. 9. Four moderately differentiated head and neck cutaneous squamous cell carcinoma-derived primary cell lines were subject to RT-qPCR, probing for OCT4 (A), NANOG (B), SOX2 (C), KLF4 (D) and c-MYC (E). ΔCT values calculated by comparing CT values of these induced-pluripotent stem cell markers to that of housekeeping gene GAPDH, with graphs displaying average ΔCT values of triplicate trials run on each sample. Positive controls are demonstrated using PC3 cells, and specificity of the probes confirmed using a no template control (NTC).

remainder represent downstream progenitor cancer cells exhibiting differing levels of stemness [16]. It is interesting that DAB IHC staining shows exclusive protein expression of NANOG on the cells within the TNs, while CISH demonstrates mRNA transcript expression throughout the TNs, the PTS and the endothelium of the microvessels within the PTS. NANOG is frequently overexpressed in SCC [37], but despite having a prominent role in regulating pluripotency, its expression is not obligatory for generation of a pluripotent phenotype [29, 30]. It is exciting to speculate that the presence of a CSC hierarchy within MDHNcSCC, with CSCs within the PTS and the endothelium of the microvessels which are transcriptionally but not translationally active for NANOG, representing the true primitive CSCs. These CSCs may differentiate to form the progenitor subpopulations within the TNs, the PTS and the endothelium of the microvessels within the PTS, although these speculations lie beyond the scope of our study.

Our findings are consistent with previous studies which observe increased expression of OCT4 in HNSCC [23]. Induction of OCT4 expression parallels an upregulation in expression of SOX2 and NANOG [23, 24]. These findings further supports our hypothesis of the presence of a CSC hierarchy, with the $OCT4^+$ cells representing the most primitive CSC subpopulation, that give rise to downstream $NANOG^+$ subpopulations. We have observed the consistent co-expression of SOX2 and OCT4 by cells within the TNs, the PTS and the endothelium of the microvessels within the PTS, which may reflect their synergistic function in maintaining pluripotency [22]. Furthermore, both DAB IHC and IF IHC staining demonstrated some nuclear expression of SOX2, which is thought to be a feature of iPSCs [22], further supporting our hypothesis of the plastic nature of the CSC hierarchy, where mature cancer cells, in the presence of a tumorigenic *niche*, may undergo de-differentiation into a primitive CSC state, by upregulation of these iPSC-associated factors.

Our findings also suggest the presence of a CSC subpopulation localized to the endothelium of microvessels within the PTS. This has similarly been observed in GB, in which CSCs have been shown to contribute to tumor angiogenesis by differentiating to form phenotypic endothelial cells which harbor GB cancer cell specific chromosomal mutations [38].

A limitation to this study is the small sample size. Future studies including larger sample size and functional work is needed to compare the expression pattern of iPSC markers with those of well- and poorly-differentiated tumors, and to the adjacent normal stem cell niches. Studies could also explore potential therapeutic targets expressed by these CSCs.

5. Conclusions

Findings of this study suggest the presence of an $OCT4^+$/$NANOG^+$/$SOX2^+$/$KLF4^+$/c-MYC^+ CSC subpopulation within the TNs, the PTS and the endothelium of microvessels within the PTS, and an $OCT4^+$/$NANOG^-$/$SOX2^+$/$KLF4^+$/c-MYC^+ subpopulation exclusively within the PTS. We speculate that these subpopulations may represent CSCs at different stages of differentiation and could be a novel therapeutic target for treatment of MDHNcSCC.

Declarations

Author contribution statement

Sabrina Koh: Performed the experiments; Analyzed and interpreted the data; Wrote the paper.

Helen Brasch: Analyzed and interpreted the data.

Jennifer de Jongh: Performed the experiments; Analyzed and interpreted the data.

Tinte Itinteang, Swee Tan: Conceived and designed the experiments; Analyzed and interpreted the data; Wrote the paper.

Funding statement

Sabrina Koh was supported by a summer scholarship from the Deane Endowment Trust.

Competing interest statement

The authors declare that the research was conducted in the absence of any commercial or financial relationships that could be construed as a potential conflict of interest. Tinte Itinteang and Swee Tan are inventors of the PCT patents Cancer Diagnosis and Therapy (PCT/NZ2015/050108), and Cancer Therapeutic (PCT/NZ2018/050006), and provisional patent application Novel Pharmaceutical Compositions for Cancer Therapy (US/62/711709).

Additional information

No additional information is available for this paper.

Acknowledgements

We thank Ms. Liz Jones and Ms. Erin Paterson of the Gillies McIndoe Research Institute for their assistance in IHC and CISH staining, and in cell culture, respectively.

References

[1] N.D.L.S. Brougham, E.R. Dennett, R. Cameron, S.T. Tan, The incidence of metastasis from cutaneous squamous cell carcinoma and the impact of its risk factors, J. Surg. Oncol. 106 (2012) 811–815.
[2] L. Lansbury, F. Bath-Hextall, W. Perkins, W. Stanton, J. Leonardi-Bee, Interventions for non-metastatic squamous cell carcinoma of the skin: systematic review and pooled analysis of observational studies, BMJ 347 (2013) f6153.
[3] N.D.L. Brougham, E.R. Dennett, S.T. Tan, Changing incidence of non-melanoma skin cancer in New Zealand, ANZ J. Surg. 81 (2011) 633–636.
[4] B.N. Harris, A. Bayoumi, S. Rao, M.G. Moore, D.G. Farwell, A.F. Bewley, Factors associated with recurrence and regional adenopathy for head and neck cutaneous squamous cell carcinoma, Otolaryngol. Head Neck Surg. 156 (2017) 863–869.
[5] N. Brougham, E.R. Dennett, S.T. Tan, Non-melanoma skin cancers in New Zealand—a neglected problem, NZ Med. J. 123 (2010) 59–65.
[6] N.D. Brougham, S.T. Tan, The incidence and risk factors of metastasis for cutaneous squamous cell carcinoma—implications on the T-classification system, J. Surg. Oncol. 110 (2014) 876–882.
[7] M. Alam, D. Ratner, Cutaneous squamous-cell carcinoma, N. Engl. J. Med. 344 (2001) 975–983.
[8] D.E. Brash, J.A. Rudolph, J.A. Simon, A. Lin, G.J. McKenna, H.P. Baden, A.J. Halperin, J. Ponten, A role for sunlight in skin cancer: UV-induced p53 mutations in squamous cell carcinoma, Proc. Natl. Acad. Sci. 88 (1991) 10124–10128.
[9] S. Ch'ng, A. Maitra, R.S. Allison, J.M. Chaplin, R.T. Gregor, R. Lea, S.T. Tan, Parotid and cervical nodal status predict prognosis for patients with head and neck metastatic cutaneous squamous cell carcinoma, J. Surg. Oncol. 98 (2008) 101–105.
[10] M.J. Veness, C.E. Palme, G.J. Morgan, High-risk cutaneous squamous cell carcinoma of the head and neck, Cancer 106 (2006) 2389–2396.
[11] R. Motley, P. Kersey, C. Lawrence, Multiprofessional guidelines for the management of the patient with primary cutaneous squamous cell carcinoma, Br. J. Dermatol. 146 (2002) 18–25.
[12] L. Sweeny, T. Zimmerman, W.R. Carroll, C.E. Schmalbach, K.E. Day, E.L. Rosenthal, Head and neck cutaneous squamous cell carcinoma requiring parotidectomy: prognostic indicators and treatment selection, Otolaryngol. Head Neck Surg. 150 (2014) 610–617.
[13] A. Bradshaw, A. Wickremsekera, S.T. Tan, L. Peng, P.F. Davis, T. Itinteang, Cancer stem cell hierarchy in glioblastoma multiforme, Front Surg. 3 (2016) 21.
[14] M. Shipitsin, K. Polyak, The cancer stem cell hypothesis: in search of definitions, markers, and relevance, Lab. Investig. 88 (2008) 459.
[15] C.T. Jordan, M.L. Guzman, M. Noble, Cancer stem cells, N. Engl. J. Med. 355 (2006) 1253–1261.
[16] S.P. Koh, A.C. Wickremesekera, T. Itinteang, S.T. Tan, Editorial: fate mapping of human glioblastoma reveals an invariant stem cell hierarchy, Transl. Cancer Res. 7 (2018) s436–s438.
[17] E. Batlle, H. Clevers, Cancer stem cells revisited, Nat. Med. 23 (2017) 1124–1134.
[18] R. Ram, H.D. Brasch, J.C. Dunne, P.F. Davis, S.T. Tan, T. Itinteang, The identification of three cancer stem cell subpopulations within moderately differentiated lip squamous cell carcinoma, Front Surg. 4 (2017) 12.
[19] H.H. Yu, T. Featherston, S.T. Tan, A.M. Chibnall, H.D. Brasch, P.F. Davis, T. Itinteang, Characterization of cancer stem cells in moderately differentiated buccal mucosal squamous cell carcinoma, Front Surg. 3 (2016) 46.
[20] R. Baillie, T. Itinteang, H.Y. Helen, H.D. Brasch, P.F. Davis, S.T. Tan, Cancer stem cells in moderately differentiated oral tongue squamous cell carcinoma, J. Clin. Pathol. 69 (2016) 742–744.
[21] A. Bradshaw, A. Wickremesekera, H.D. Brasch, A.M. Chibnall, P.F. Davis, S.T. Tan, T. Itinteang, Cancer stem cells in glioblastoma multiforme, Front Surg. 3 (2016) 48.
[22] B. van Schaijik, P.F. Davis, A.C. Wickremesekera, S.T. Tan, T. Itinteang, Subcellular localisation of the stem cell markers OCT4, SOX2, NANOG, KLF4 and c-MYC in cancer: a review, J. Clin. Pathol. 71 (2018) 88–91.
[23] B.S. Koo, S.H. Lee, J.M. Kim, S. Huang, S.H. Kim, Y.S. Rho, W.J. Bae, H.J. Kang, Y.S. Kim, J.H. Moon, Y.C. Lim, Oct4 is a critical regulator of stemness in head and neck squamous carcinoma cells, Oncogene 34 (2015) 2317–2324.
[24] D. Racila, M. Winter, M. Said, A. Tomanek-Chalkley, S. Wiechert, R.L. Eckert, J.R. Bickenbach, Transient expression of OCT4 is sufficient to allow human keratinocytes to change their differentiation pathway, Gene Ther. 18 (2011) 294.
[25] S. Boumahdi, G. Driessens, G. Lapouge, S. Rorive, D. Nassar, M. Le Mercier, B. Delatte, A. Caauwe, S. Lenglez, E. Nkusi, S. Brohee, I. Salmon, C. Dubois, V. del Marmol, F. Fuks, B. Beck, C. Blanpain, SOX2 controls tumour initiation and cancer stem-cell functions in squamous-cell carcinoma, Nature 511 (2014) 246–250.
[26] Y.-J. Chen, C.-Y. Wu, C.-C. Chang, C.-J. Ma, M.-C. Li, C.-M. Chen, Nuclear Krüppel-like factor 4 expression is associated with human skin squamous cell carcinoma progression and metastasis, Cancer Biol. Ther. 7 (2014) 777–782.
[27] K.W. Foster, Z. Liu, C.D. Nail, X. Li, T.J. Fitzgerald, S.K. Bailey, A.R. Frost, I.D. Louro, T.M. Townes, A.J. Paterson, J.E. Kudlow, S.M. Lobo-Ruppert, J.M. Ruppert, Induction of KLF4 in basal keratinocytes blocks the proliferation-differentiation switch and initiates squamous epithelial dysplasia, Oncogene 24 (2005) 1491–1500.
[28] S. Pelengaris, T. Littlewood, M. Khan, G. Elia, G. Evan, Reversible activation of c-Myc in skin: induction of a complex neoplastic phenotype by a single oncogenic lesion, Mol. Cell 3 (1999) 565–577.
[29] K. Takahashi, K. Tanabe, M. Ohnuki, M. Narita, T. Ichisaka, K. Tomoda, S. Yamanaka, Induction of pluripotent stem cells from adult human fibroblasts by defined factors, Cell 131 (2007) 861–872.
[30] J. Yu, M.A. Vodyanik, K. Smuga-Otto, J. Antosiewicz-Bourget, J.L. Frane, S. Tian, J. Nie, G.A. Jonsdottir, V. Ruotti, R. Stewart, I.I. Slukvin, J.A. Thomson, Induced pluripotent stem cell lines derived from human somatic cells, Science 318 (2007) 1917–1920.
[31] T. Itinteang, H.D. Brasch, S.T. Tan, D.J. Day, Expression of components of the renin–angiotensin system in proliferating infantile haemangioma may account for the propranolol-induced accelerated involution, J. Plast. Reconstr. Aesthet. Surg. 64 (2011) 759–765.
[32] E.M. Tan, D.A. Chudakova, P.F. Davis, H.D. Brasch, T. Itinteang, S.T. Tan, Characterisation of subpopulations of myeloid cells in infantile haemangioma, J. Clin. Pathol. 68 (2015) 571–574.
[33] E. Vlashi, F. Pajonk, Cancer stem cells, cancer cell plasticity and radiation therapy, Semin. Cancer Biol. 31 (2015) 28–35.
[34] I. Sancho-Martinez, E. Nivet, Y. Xia, T. Hishida, A. Aguirre, A. Ocampo, L. Ma, R. Morey, M.N. Krause, A. Zembrzycki, Establishment of human iPSC-based models for the study and targeting of glioma initiating cells, Nat. Commun. 7 (2016) 10743.
[35] C.A. Hey, K.B. Saltökova, H.C. Bisgaard, L.B. Møller, Comparison of two different culture conditions for derivation of early hiPSC, Cell Biol. Int. 42 (2018) 1467–1473.
[36] X. Lan, D.J. Jörg, F.M.G. Cavalli, L.M. Richards, L.V. Nguyen, R.J. Vanner, P. Guilhamon, L. Lee, M.M. Kushida, D. Pellacani, N.I. Park, F.J. Coutinho, H. Whetstone, H.J. Selvadurai, C. Che, B. Luu, A. Carles, M. Moksa, N. Rastegar, R. Head, S. Dolma, P. Prinos, M.D. Cusimano, S. Das, M. Bernstein, C.H. Arrowsmith, A.J. Mungall, R.A. Moore, Y. Ma, M. Gallo, M. Lupien, T.J. Pugh, M.D. Taylor, M. Hirst, C.J. Eaves, B.D. Simons, P.B. Dirks, Fate mapping of human glioblastoma reveals an invariant stem cell hierarchy, Nature 549 (2017) 227–232.
[37] A.R. Palla, D. Piazzolla, N. Alcazar, M. Canamero, O. Grana, G. Gomez-Lopez, O. Dominguez, M. Duenas, J.M. Paramio, M. Serrano, The pluripotency factor NANOG promotes the formation of squamous cell carcinomas, Sci. Rep. 5 (2015) 10205.
[38] L. Ricci-Vitiani, R. Pallini, M. Biffoni, M. Todaro, G. Invernici, T. Cenci, G. Maira, E.A. Parati, G. Stassi, L.M. Larocca, R. De Maria, Tumour vascularization via endothelial differentiation of glioblastoma stem-like cells, Nature 468 (2010) 824–828.